Light trapping in periodically textured amorphous silicon thin film solar cells using realistic interface morphologies

Vladislav Jovanov,[1] Ujwol Palanchoke,[1] Philipp Magnus,[2] Helmut Stiebig,[2] Jürgen Hüpkes,[3] Porponth Sichanugrist,[4] Makoto Konagai,[4,5] Samuel Wiesendanger,[6] Carsten Rockstuhl,[6] and Dietmar Knipp[1,*]

[1] *Research Center for Functional Materials and Nanomolecular Science, Electronic Devices and Nanophotonics Laboratory, Jacobs University Bremen, Bremen, Germany*
[2] *Malibu GmbH and Co.KG, Bielefeld, Germany*
[3] *Institut für Energie-undKlimaforschung, IEK5—Photovoltaik, Forschungszentrum Jülich, Germany*
[4] *Department of Physical Electronics, Tokyo Institute of Technology, Tokyo, Japan*
[5] *Photovoltaics Research Center (PVREC), Tokyo Institute of Technology, Tokyo, Japan*
[6] *Institute of Condensed Matter Theory and Optics, Friedrich-Schiller-Universität, Jena, Germany*
[*] *d.knipp@jacobs-university.de*

Abstract: The influence of realistic interface morphologies on light trapping in amorphous silicon thin-film solar cells with periodic surface textures is studied. Realistic interface morphologies are obtained by a 3D surface coverage algorithm using the substrate morphology and layer thicknesses as input parameters. Finite difference time domain optical simulations are used to determine the absorption in the individual layers of the thin-film solar cell. The influence of realistic interface morphologies on light trapping is determined by using solar cells structures with the same front and back contact morphologies as a reference. Finally the optimal surface textures are derived.

OCIS codes: (350.6050) Solar energy; (310.6845) Thin film devices and applications; (240.5770) Roughness; (240.6700) Surfaces.

References and links

1. M. Konagai, "Present status and future prospects of silicon thin-film solar cells," Jpn. J. Appl. Phys. **50**, 030001 (2011).
2. M. Zeman, R. A. C. M. M. van Swaaij, J. W. Metselaar, and R. E. I. Schropp, "Optical modeling of a-Si:H solar cells with rough interfaces: effect of back contact and interface roughness," J. Appl. Phys. **88**(11), 6436–6443 (2000).
3. J. Müller, B. Rech, J. Springer, and M. Vanecek, "TCO and light trapping in silicon thin film solar cells," Sol. Energy **77**(6), 917–930 (2004).
4. A. Hongsingthong, T. Krajangsang, B. Janthong, P. Sichanugrist, and M. Konagai, "Effect of high-haze zinc oxide films fabricated on soda-lime glass substrate for thin-film silicon solar cells," 37th IEEE Photovoltaic Specialists Conference, 000791–000794 (2011).
5. J. Krc, B. Lipovsek, M. Bokalic, A. Campa, T. Oyama, M. Kambe, T. Matsui, H. Sai, M. Kondo, and M. Topic, "Potential of thin-film silicon solar cells by using high haze TCO superstrates," Thin Solid Films **518**(11), 3054–3058 (2010).
6. S. Faÿ, U. Kroll, C. Bucher, E. Vallat-Sauvain, and A. Shah, "Low pressure chemical vapour deposition of ZnO layers for thin-film solar cells: temperature-induced morphological changes," Sol. Energy Mater. Sol. Cells **86**(3), 385–397 (2005).
7. J. Meier, J. Spitznagel, U. Kroll, C. Bucher, S. Faÿ, T. Moriarty, and A. Shah, "Potential of amorphous and microcrystalline silicon solar cells," Thin Solid Films **451–452**, 518–524 (2004).
8. C. Battaglia, C.-M. Hsu, K. Söderström, J. Escarré, F.-J. Haug, M. Charrière, M. Boccard, M. Despeisse, D. T. L. Alexander, M. Cantoni, Y. Cui, and C. Ballif, "Light trapping in solar cells: can periodic beat random?" ACS Nano **6**(3), 2790–2797 (2012).
9. C. Battaglia, J. Escarré, K. Söderström, M. Charriére, M. Despeisse, F.-J. Haug, and C. Ballif, "Nanomoulding of transparent zinc oxide electrodes for efficient light trapping in solar cells," Nat. Photonics **5**(9), 535–538 (2011).
10. W. J. Nam, L. Ji, T. L. Benanti, V. V. Varadan, S. Wagner, Q. Wang, W. Nemeth, D. Neidich, and S. J. Fonash, "Incorporation of a light and carrier collection management nano-element array into superstrate a-Si:H solar cells," Appl. Phys. Lett. **99**(7), 073113 (2011).

#188123 - $15.00 USD Received 1 Apr 2013; revised 29 Apr 2013; accepted 12 May 2013; published 22 May 2013

11. S. Solntsev, O. Isabella, D. Caratelli, and M. Zeman, "Thin-film silicon solar cells on 1-D periodic gratings with nonconformal layers: optical analysis," IEEE J. Photovoltaics **3**(1), 46–52 (2013).
12. A. Naqavi, K. Söderström, F. J. Haug, V. Paeder, T. Scharf, H. P. Herzig, and C. Ballif, "Understanding of photocurrent enhancement in real thin film solar cells: towards optimal one-dimensional gratings," Opt. Express **19**(1), 128–140 (2011).
13. U. W. Paetzold, E. Moulin, B. E. Pieters, R. Carius, and U. Rau, "Design of nanostructured plasmonic back contacts for thin-film silicon solar cells," Opt. Express **19**(S6 Suppl 6), A1219–A1230 (2011).
14. C.-M. Hsu, C. Battaglia, C. Pahud, Z. Ruan, F.-J. Haug, S. Fan, C. Ballif, and Y. Cui, "High-efficiency amorphous silicon solar cell on a periodic nanocone back reflector," Adv. Energy Mater. **2**(6), 628–633 (2012).
15. F.-J. Haug, T. Söderström, M. Python, V. Terrazzoni-Daudrix, X. Niquille, and C. Ballif, "Development of micromorph tandem solar cells on flexible low-cost plastic substrates," Sol. Energy Mater. Sol. Cells **93**(6-7), 884–887 (2009).
16. H. Sai, H. Fujiwara, M. Kondo, and Y. Kanamori, "Enhancement of light trapping in thin-film hydrogenated microcrystalline Si solar cells using back reflectors with self-ordered dimple pattern," Appl. Phys. Lett. **93**(14), 143501 (2008).
17. H. Sai, H. Jia, and M. Kondo, "Impact of front and rear texture of thin-film microcrystalline silicon solar cells on their light trapping properties," J. Appl. Phys. **108**(4), 044505 (2010).
18. V. E. Ferry, A. Polman, and H. A. Atwater, "Modeling light trapping in nanostructured solar cells," ACS Nano **5**(12), 10055–10064 (2011).
19. D. Madzharov, R. Dewan, and D. Knipp, "Influence of front and back grating on light trapping in microcrystalline thin-film silicon solar cells," Opt. Express **19**(S2 Suppl 2), A95–A107 (2011).
20. R. Dewan, J. I. Owen, D. Madzharov, V. Jovanov, J. Hüpkes, and D. Knipp, "Analyzing nanotextured transparent conductive oxides for efficient light trapping in silicon thin film solar cells," Appl. Phys. Lett. **101**(10), 103903 (2012).
21. U. Palanchoke, V. Jovanov, H. Kurz, P. Obermeyer, H. Stiebig, and D. Knipp, "Plasmonic effects in amorphous silicon thin film solar cells with metal back contacts," Opt. Express **20**(6), 6340–6347 (2012).
22. J. Lacombe, O. Sergeev, K. Chakanga, K. von Maydell, and C. Agert, "Three dimensional optical modeling of amorphous silicon thin film solar cells using the finite-difference time-domain method including real randomly surface topographies," J. Appl. Phys. **110**(2), 023102 (2011).
23. R. Biswas and C. Xu, "Nano-crystalline silicon solar cell architecture with absorption at the classical 4n2 limit," Opt. Express **19**(S4 Suppl 4), A664–A672 (2011).
24. C. Haase and H. Stiebig, "Thin-film silicon solar cells with efficient periodic light trapping texture," Appl. Phys. Lett. **91**(6), 061116 (2007).
25. U. Palanchoke, V. Jovanov, H. Kurz, R. Dewan, P. Magnus, H. Stiebig, and D. Knipp, "Influence of back contact roughness on light trapping and plasmonic losses of randomly textured amorphous silicon thin film solar cells," Appl. Phys. Lett. **102**(8), 083501 (2013).
26. V. Jovanov, U. Planchoke, P. Magnus, H. Stiebig, and D. Knipp, "Influence of back contact morphology on light trapping and plasmonic effects in microcrystalline silicon single junction and micromorph tandem solar cells," Sol. Energy Mater. Sol. Cells **110**, 49–57 (2013).
27. V. Jovanov, X. Xu, S. Shrestha, M. Schulte, J. Hüpkes, M. Zeman, and D. Knipp, "Influence of interface morphologies on amorphous silicon thin film solar cells prepared on randomly textured substrates," Sol. Energy Mater. Sol. Cells **112**, 182–189 (2013).
28. S. Eckhardt, C. Sachse, and A. F. Lasagni, "Light Management in Transparent Conducting Oxides by Direct Fabrication of Periodic Surface Arrays," Phys. Procedia **41**, 545–550 (2013).
29. F.-J. Haug, T. Söderström, O. Cubero, V. Terrazzoni-Daudrix, and C. Ballif, "Plasmonic absorption in textured silver back reflectors of thin film solar cells," J. Appl. Phys. **104**(6), 064509 (2008).
30. R. A. Street, *Hydrogenated Amorphous Silicon*, Cambridge University Press, (1991), Chap. **2**.
31. C. C. Tsai, J. C. Knights, G. Chang, and B. Wacker, "Film formation mechanisms in the plasma deposition of hydrogenated amorphous silicon," J. Appl. Phys. **59**(8), 2998–3001 (1986).

1. Introduction

To maximize the energy conversion efficiency of silicon thin-film solar cells the optical and electrical properties have to be optimized. Amorphous silicon films exhibit a high electric defect density and low charge carrier diffusion length. Therefore, best electrical performances of low temperature amorphous silicon solar cells are achieved if the solar cell thickness is limited to a couple of hundreds of nanometers [1–4]. For such thin solar cells, light trapping is imperative to increase the short circuit currents. Light trapping is typically introduced by nanotexturing the front (p-i-n configuration) or the back contact (n-i-p configuration) of the solar cells [1–18]. Nanotextures scatter/diffract the incident light so that the optical path length and light absorption within the active layer of the solar cell is increased. Efficient light trapping is achieved when light absorption is improved for complete absorption spectrum of the active material.

Experimental results and optical simulations show that solar cells with textured front and back contact exhibit improved light trapping compared to solar cells with only one textured

#188123 - $15.00 USD Received 1 Apr 2013; revised 29 Apr 2013; accepted 12 May 2013; published 22 May 2013

contact [17,19]. Optimal nanotextures for the front and back contact are different. The optimal textures for the front contact are designed to reduce reflection losses and increase scattering/diffraction of the incident light [1–10]. On the other hand, optimal back contact textures should reduce absorption in the metal back reflector and efficiently scatter/diffract the reflected light [11–18]. Efficient light trapping is typically realized by optimizing nanotextures for only one contact of the solar cell. Texturing of the other contact is achieved by the deposition of the solar cell layers. The nanotextures propagate through the thin-film solar cell influencing the textures and light trapping properties of the other contact.

Optical simulation tools are often used to analyze wave propagation within thin-film solar cells and derive optimal light trapping structures [10–13,18–26]. A good optical model of the silicon thin-film solar cell requires an accurate description of the front and the back contact morphology. Since amorphous silicon solar cells are very thin, it is commonly assumed that the front and back contact morphologies are the same [18–25]. However, experimental measurements show significant differences between the front and back contact textures [1,2,8–12,14,15,17,27]. A realistic description of the interface morphologies is necessary to optimize the quantum efficiency and short circuit current of the solar cells [10–12,27]. Furthermore, obtaining realistic interface morphologies is crucial when describing the optics of solar cells on double textured substrates or radial nanowire solar cells [4,5,10]. A typical approach to determine realistic interface morphologies is by using cross-sectional scanning electron microscopy (SEM) images [8–12,14,15,17]. However, cross-sectional SEM images can record interface morphologies only as a function of one dimension and this approach is accurate for substrates such as line-gratings or periodically textured substrates with radial symmetry [8–12,16]. In this manuscript, we investigate the influence of realistic interface morphologies on light trapping of amorphous silicon thin-film solar cells in superstate (p-i-n) configuration with periodic surface textures. Realistic interface morphologies are obtained by a surface coverage algorithm [27]. The model to obtain realistic interface morphologies is described in Section 2. Optical simulation tools and simulated structures are presented in Section 3. The influence of surface texture on the short circuit current and optical losses is presented in Section 4, followed by summary in Section 5.

2. Modeling the interface morphology

Randomly textured transparent conductive oxides (TCO) are commonly used to achieve light trapping in superstate (p-i-n) configuration solar cells [1–7]. However, recent studies have shown that solar cells prepared on periodic surface textures exhibit comparable conversion efficiencies exceeding 10% [8,9,14]. The randomly textured TCO are realized by wet etching of sputtered zinc oxide (ZnO), low pressure chemical vapor deposition of ZnO films or by atmospheric pressure chemical vapor deposition of tin oxide films [1–7]. Fabrication of periodic substrates can be achieved by texturing of the glass substrate or by direct patterning of the TCO films [8,9,14,28]. In general, the front contact textures can be described either as pyramid or crater-like features. The front contact textures propagate through the solar cell and determine the morphology of the back contact. The optical losses in the metal back reflector and consequently the short circuit current depend on the optical properties of the dielectric/metal interface and the back contact morphology [3,13,21,25,26,29]. A ZnO interlayer introduced between the amorphous silicon p-i-n diode and the metal reflector decreases optical losses in the back contact [Figs. 1(c) and 1(d)]. However, it has been shown that the back contact morphology has a larger influence on light trapping than the optical properties of the dielectric/metal interface [25,26]. Hence, an accurate description of the back contact morphology is required for further investigation and optimization of light trapping.

Low temperature amorphous silicon solar cells are typically deposited by plasma enhanced chemical vapor deposition (PECVD). The growth conditions of PECVD processes range from chemical vapor deposition (CVD) to physical vapor deposition (PVD) conditions [30,31]. Good electrical properties of the amorphous silicon solar cells are achieved when films are grown under CVD-like growth conditions [30,31]. CVD-like growth conditions exhibit low sticking coefficients and the surface coverage of amorphous silicon films is

#188123 - $15.00 USD Received 1 Apr 2013; revised 29 Apr 2013; accepted 12 May 2013; published 22 May 2013

excellent. Consequently, amorphous silicon films are uniform and without voids, and exhibit low density of electronic defects. Taking these considerations into account, it can be assumed that amorphous silicon grows in the direction of local surface normal [Fig. 1(b)]. By using this approach, a very good agreement between experimentally measured and simulated surface morphologies is demonstrated for amorphous silicon films deposited on randomly textured substrates [27].

Figures 1(a) and 1(b) schematically show the standard and realistic approach to model interface morphologies of amorphous silicon film deposited on a textured substrate. For the standard interface morphologies it is assumed that the silicon film grows in the direction of the glass substrate [Fig. 1(a)]. If the thickness of the solar cell or silicon film is smaller than the lateral dimensions of the front contact textures (dashed lines), the realistic description of the surface morphology exhibit only smaller differences from the front contact textures and the standard model provides a good description. If the thickness of the solar cell is comparable with the lateral dimensions of the front textures (full lines), the differences between the realistic and standard interface morphologies are significant. In this study, we investigated substrates with periodic surface textures. Periodic textures of the TCO substrate were defined by a pyramid shape with a square shaped base. The pyramid is described by the period and the height, which also define the opening angle (α) [Fig. 1(d)]. The period of the pyramid was varied from 50 to 500 nm with steps of 50 nm, while the height was varied from 0 to 150 nm with steps of 30 nm.

Figures 1(c) and 1(d) exhibit cross sections of amorphous silicon solar cells with interface morphologies according to the standard and realistic interface description. For the standard structure, the front contact textures propagate unchanged through the solar cell layers [Fig. 1(c)]. Consequently, the root mean square (rms) roughness of the back contact is the same as for the front contact. The roughness of the pyramid texture is given by:

$$R_{q-pyr} = \frac{H}{3\sqrt{2}} \tag{1}$$

where H is the height of the pyramid. The back contact morphology for the realistic model

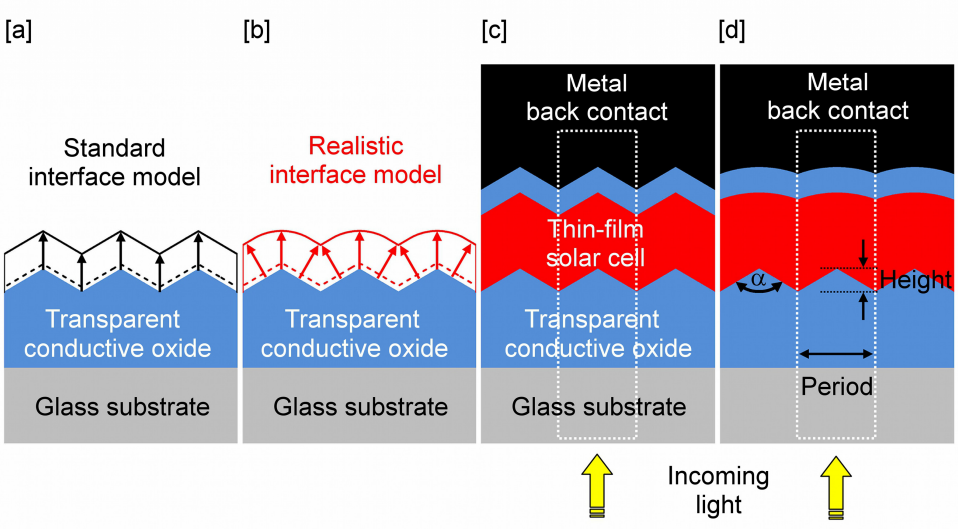

Fig. 1. Silicon film formation in the direction of (a) the glass substrate normal and (b) the local surface normal. Cross section of amorphous silicon solar cells with periodic surface textures using (c) standard interface morphologies and (d) realistic interface morphologies.

[Fig. 1(d)] was determined by a surface coverage algorithm [27]. The surface coverage algorithm calculates the interface morphology by using the front contact textures and layer

#188123 - $15.00 USD Received 1 Apr 2013; revised 29 Apr 2013; accepted 12 May 2013; published 22 May 2013

thickness (nominal value) as input data assuming film formation in the direction of the local surface normal. Consequently, for realistic structures the back contact morphology and roughness are different from the front contact [Fig. 1(d)]. The back contact roughness as a function of the solar cell thickness for different periods and heights of the pyramid textures is shown in Fig. 2. For the standard solar cell structure, the back contact roughness only depends on the height of the pyramid (dashed lines). For solar cells with realistic interface morphologies, the roughness of the back contact decreases with increasing solar cell thickness (full lines). The film roughness depends on the height and period of the pyramid [Figs. 2(a) and 2(b)].

The thickness of the solar cell layers is also influenced by the film formation on the textured substrate. For the standard solar cell model, the thickness of all solar cell layers is equal to the nominal thickness since there is no change in surface textures. For the realistic structure, the interface morphology changes and consequently the film thickness is different from the nominal film thickness. The film thickness is equal to the nominal film thickness only at the peak of the pyramid. Everywhere else, the film thickness is higher than the nominal film thickness. The thickness increase is important mainly for the p- and i-layer of the solar cell [27]. The thickness of the p-layer determines the optical losses in the p-layer,

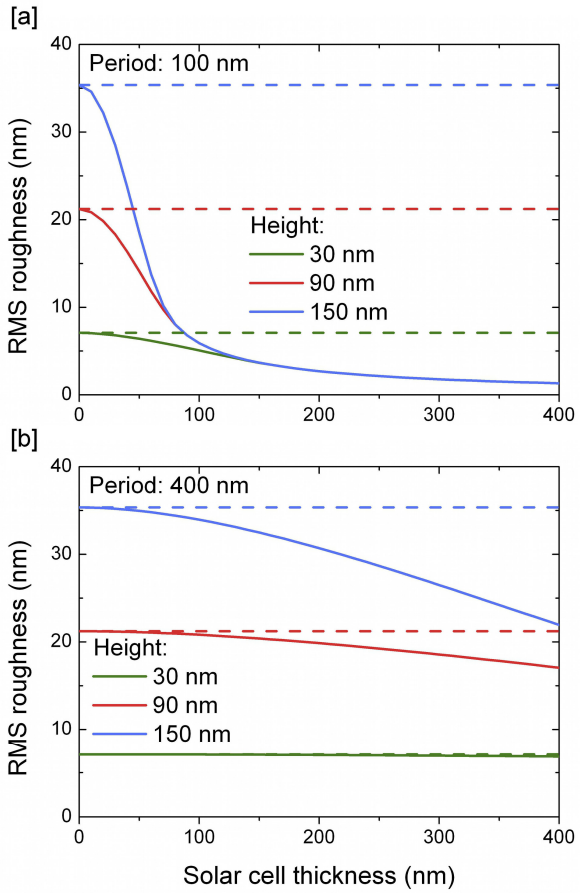

Fig. 2. Back contact roughness as a function of a solar cell thickness for different pyramid heights and period of a (a) 100 nm and (b) 400 nm. Back contact roughness for standard solar cell structures is presented with dashed lines.

#188123 - $15.00 USD Received 1 Apr 2013; revised 29 Apr 2013; accepted 12 May 2013; published 22 May 2013

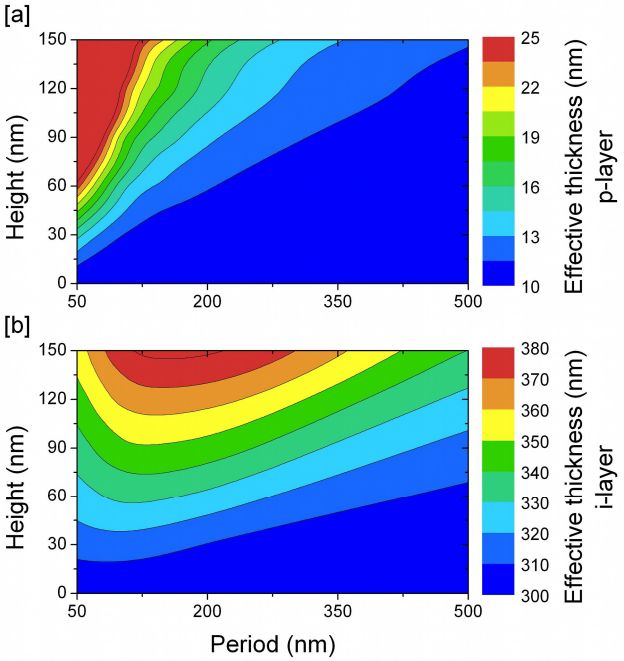

Fig. 3. Effective thickness of the solar cell (a) p-layer with nominal thickness of 10 nm and (b) i-layer with nominal thickness of 300 nm as a function of pyramid dimensions.

while the quantum efficiency of the solar cell depends upon the thickness of the i-layer. In this study, nominal thicknesses for the p- and i-layer were chosen to be 10 nm and 300 nm, respectively, which is consistent with typical amorphous silicon solar cells. The surface coverage algorithm was used to calculate interface morphologies of the p- and i-layer for all period and height combinations of the pyramid texture. To determine the influence of the interface morphology on the film thickness, the effective thickness of the layers (d_{eff}) was introduced. The effective thickness can be calculated by:

$$d_{eff} = \frac{V_{layer}}{P^2} \tag{2}$$

where V_{layer} is the volume of the specific solar cell layer and P is the period of the pyramid texture. The effective thickness of the p- and i-layer as a function of the period and height of the pyramid texture is presented in Fig. 3.

Figure 3(a) exhibits the effective thickness of the p-layer for the realistic solar cell structure. The effective thickness of the p-layer is larger than 25 nm if the opening angle of the pyramid texture is smaller than 50°. As the opening angle increases, the effective thickness reduces. If the opening angle is larger than 120°, the effective thickness is close to the nominal thickness of 10 nm. The effective thickness of the i-layer is presented in the Fig. 3(b). In this case, the effective thickness increases with increased height of the pyramid. The effective thickness is highest for a period of 150 nm. By increasing or decreasing the pyramid period, the effective thickness is reduced. This effect is caused by the fact that the effective thickness of the i-layer is a function of the p-layer thickness, the i-layer thickness and the pyramid dimensions. For the investigated periods and heights of the pyramid texture, the highest effective thickness of the i-layer is close to 380 nm.

3. Optical simulations

The influence of the interface morphology on light-trapping was determined by optical simulations. In this study, finite difference time domain (FDTD) method was used to

#188123 - $15.00 USD Received 1 Apr 2013; revised 29 Apr 2013; accepted 12 May 2013; published 22 May 2013

numerically solve Maxwell's equations in three dimensions. The optical simulations were used to analyze electromagnetic wave propagation in solar cell structures and to determine the absorption for the individual layers. The front contact of the simulated solar cells consists of a pyramid texture and 420 nm thick layer of tin oxide coated on a glass substrate [Figs. 4 and 6]. The amorphous silicon diode is composed of a p-doped, an intrinsic and an n-doped layer with nominal thicknesses of 10 nm, 300 nm and 10 nm, respectively. The back contact consists of a 100 nm (nominal value) thick ZnO interlayer followed by a silver (Ag) back reflector. The interface morphologies of the simulated solar cell structures were described by the standard and the realistic approach. The standard solar cell structures were used as a reference. To compare results directly, the simulation settings were the same for all structures. Mesh size in x- and y-direction was set to 10 nm. In z-direction, the mesh size for bulk material regions was not larger than 10 nm. For the interface regions, the mesh size was set to 2 nm. The input light source was set to be a plane wave with normal incidence relative to the

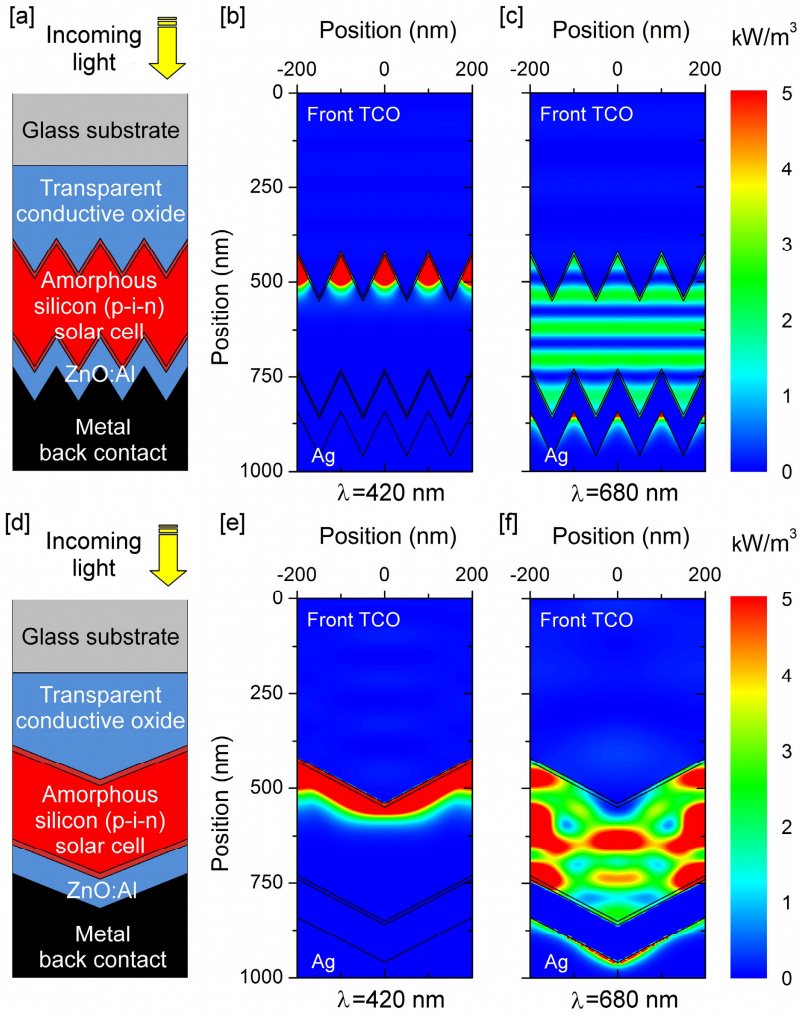

Fig. 4. (a) Cross section of amorphous silicon solar cell with standard interfaces for period of 100 nm and height of 120 nm. Corresponding power loss profiles for wavelength of (b) 420 nm and (c) 680 nm. (d) Cross section of amorphous silicon solar cell with standard interfaces for period of 400 nm and height of 120 nm. Corresponding power loss profiles for wavelengths of (e) 420 nm and (f) 680 nm.

#188123 - $15.00 USD Received 1 Apr 2013; revised 29 Apr 2013; accepted 12 May 2013; published 22 May 2013

simulated structure. The wavelength range of the input source was varied from 300 nm to 800 nm with 10 nm steps. The glass substrate was described as a non-absorbing dielectric material with refractive index of 1.5. The optical constants of the other materials used in the simulations were determined by experimental measurements and represented analytically in the FDTD solver. The fitting error was minimized by dividing the complete wavelength range into two smaller ranges: 300-590 nm and 600-800 nm [11,26]. Simulations were carried out for the all period and height combinations of the pyramid texture.

Figure 4 exhibits the influence of the pyramid period on the light trapping in standard solar cell structures. Figures 4(a) and 4(d) show cross sections of the standard solar cells. The pyramid period for the structure in Fig. 4(a) is 100 nm and for the structure in Fig. 4(d) is 400 nm. The height of the pyramid texture is 120 nm for both structures. Corresponding power loss profiles for the structure in Fig. 4(a) are presented in Figs. 4(b) and 4(c). The power loss profiles in Figs. 4(e) and 4(f) correspond to the structure in Fig. 4(d). The power loss profiles were obtained for wavelengths of 420 nm [Figs. 4(b) and 4(e)] and 680 nm [Figs. 4(c) and 4(f)]. Figures 4(b) and 4(e) show that shorter wavelengths get absorbed in the front of the solar cell. For longer wavelengths, smaller periods act as an effective refractive index regions and there is no scattering/diffraction of the light [Fig. 4(c)]. The larger pyramid periods effectively scatter/diffract longer wavelength light and better light trapping is achieved [Fig. 4(f)].

The quantum efficiencies and reflections for the standard structures are shown in Figs. 5(a) and 5(b), respectively. The quantum efficiencies are calculated assuming that only electron/hole pairs generated in the i-layer contribute to the overall current and that all charge carriers are collected. For shorter wavelengths, the reflection of the solar cell structure with a period of 100 nm is lower compared to period of 400 nm [Fig. 5(b)]. Consequently, the quantum efficiency is increased compared to larger periods [Fig. 5(a)]. On the other hand, in the longer wavelength region the quantum efficiency is higher for larger periods due to the better scattering/diffraction properties of the back contact. Based on the results for the standard structures, it can be concluded that smaller periods achieve better incoupling of shorter wavelengths, while larger periods are better for light trapping of longer wavelengths.

The influence of the pyramid period on the light trapping in solar cells with realistic interface morphologies is presented in Fig. 6. The same pyramid periods and heights are presented as for standard structures. Cross sections of the solar cells with realistic interfaces [Figs. 6(a) and 6(d)] show that the thickness of solar cell layers and back contact morphology depends on the pyramid period. Power loss profiles for wavelengths of 420 nm and 680 nm are shown in Figs. 6(b) and 6(c) for period of 100 nm and Figs. 6(e) and 6(f) for period of 400

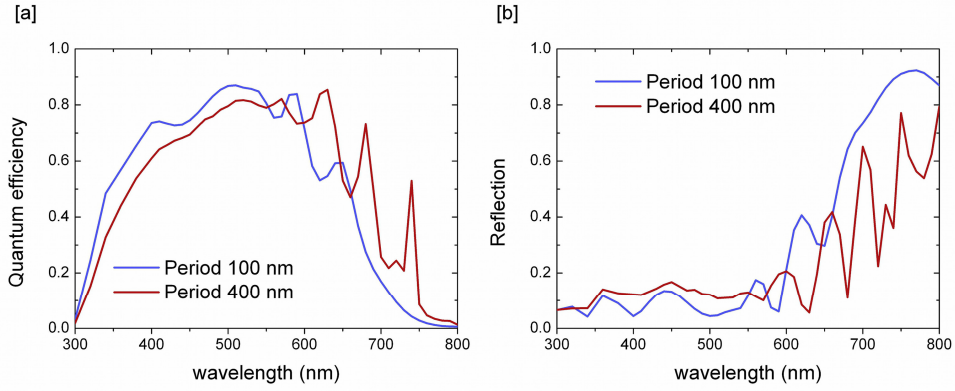

Fig. 5. Quantum efficiencies of standard solar cell structures for pyramid height of 120 nm and periods of 100 nm and 400 nm.

#188123 - $15.00 USD Received 1 Apr 2013; revised 29 Apr 2013; accepted 12 May 2013; published 22 May 2013

nm. For a period of 100 nm, the thickness of the p-layer is significantly increased and the absorption losses in the p-layer are high. For longer wavelengths, the back contact losses are reduced compared to the standard structure due to the almost flat back contact morphology. The reduced absorption in the back contact results does not result in an increased quantum efficiency since there is no efficient scattering of the reflected light. For larger periods, the effective thickness of the p-layer is comparable to the nominal thickness. Therefore, the power loss profile for shorter wavelengths is similar to the corresponding standard structure. The back contact morphology is smoother compared to the standard structure and the absorption losses for longer wavelengths at the ZnO/Ag interface are reduced. On the other hand, the back contact roughness is still high enough to efficiently scatter/diffract reflected light and the absorption of the light in the i-layer is increased.

The quantum efficiencies and reflections for the realistic structures are shown in Figs. 7(a) and 7(b), respectively. The quantum efficiencies exhibit different trends compared to the

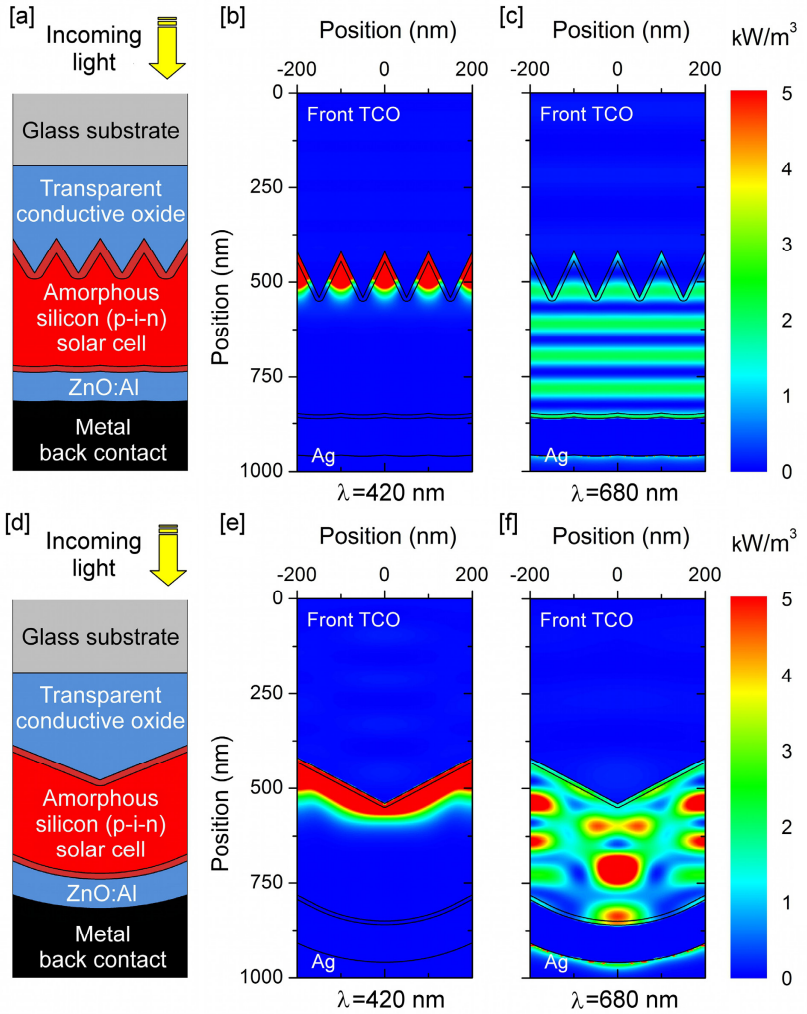

Fig. 6. (a) Cross section of realistic amorphous silicon solar cell for period of 100 nm and height 120 nm. Corresponding power loss profiles for wavelength of (b) 420 nm and (c) 680 nm. (d) Cross section of amorphous silicon solar cell with standard interfaces for pyramid period of 400 nm and height 120 nm. Corresponding power loss profiles for wavelength of (e) 420 nm and (f) 680 nm.

#188123 - $15.00 USD Received 1 Apr 2013; revised 29 Apr 2013; accepted 12 May 2013; published 22 May 2013

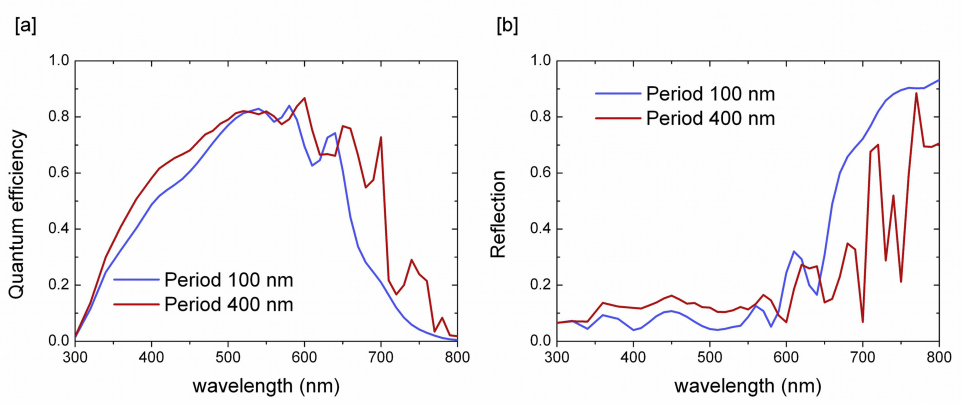

Fig. 7. Quantum efficiencies of realistic solar cell structures for pyramid height of 120 nm and periods of 100 nm and 400 nm.

standard structures. The realistic structure with period of 400 nm exhibits higher quantum efficiency compared to period of 100 nm for all wavelengths. For shorter wavelengths, the reflection is smaller for period of 100 nm and good light incoupling is achieved [Fig. 7(b)]. However, the quantum efficiency for period of 100 nm is smaller due to the thicker p-layer [Fig. 7(a)]. For longer wavelengths, period of 400 nm achieves better light trapping compared to period of 100 nm. The presented results show that accurate description of interface morphology is important for better analysis and understanding of light trapping structures.

4. Optical losses and light trapping

The interface morphology influences the quantum efficiency and the absorption of light in the individual layers of the p-i-n diode and the metal back reflector. In order to determine the influence of the realistic interface morphologies on light trapping, the short circuit currents were calculated for all period and height combinations of the pyramid texture. The optical losses were expressed as current losses. The front contact losses represent absorption of the light in the front TCO layer and the p-layer. The back contact losses are the total absorption in the n-layer, the ZnO interlayer and the metal back reflector. The short circuit currents and the optical losses as a function of the period and the height are presented in Fig. 8.

Figure 8 exhibits the interplay between light trapping and optical losses for standard and realistic solar cell structures. The standard structures exhibit relatively low front contact losses [Fig. 8(a)] compared to the front contact losses of realistic structures [Fig. 8(b)]. The front contact losses for realistic structures are highest where the effective thickness of the p-layer is larger than 25 nm as shown in Fig. 3(a). The front contact losses for the standard and the realistic structures are similar for larger periods where the increase of p-layer thickness is smaller. The front contact losses have little influence on the short circuit current for the standard structures [Fig. 8(c)]. On the other hand, for the realistic structures high front contact losses result in low short circuit currents for smaller periods [Fig. 8(d)]. To avoid high front contact losses for smaller periods, thinner p-layers can be used. Figures 8(c) and 8(d) show that the optimal light trapping dimensions are the same for the standard and the realistic structures. However, the short circuit currents for realistic structures are higher. This is influenced mainly by the back contact morphology. The roughness of the back contact morphology for realistic structures is smaller and results in lower back contact losses. At the same time, the back contact roughness is still large enough to efficiently scatter/diffract reflected light. The back contact losses for standard and realistic structures are shown in Figs. 8(e) and 8(f), respectively. There is a tradeoff between back contact losses and short circuit currents. For the standard structures, back contact absorption is higher for optimal light trapping dimensions and the short circuits are reduced. For the same optimal textures, the realistic structures exhibit only minor back contact losses and the short circuit currents are

#188123 - $15.00 USD Received 1 Apr 2013; revised 29 Apr 2013; accepted 12 May 2013; published 22 May 2013

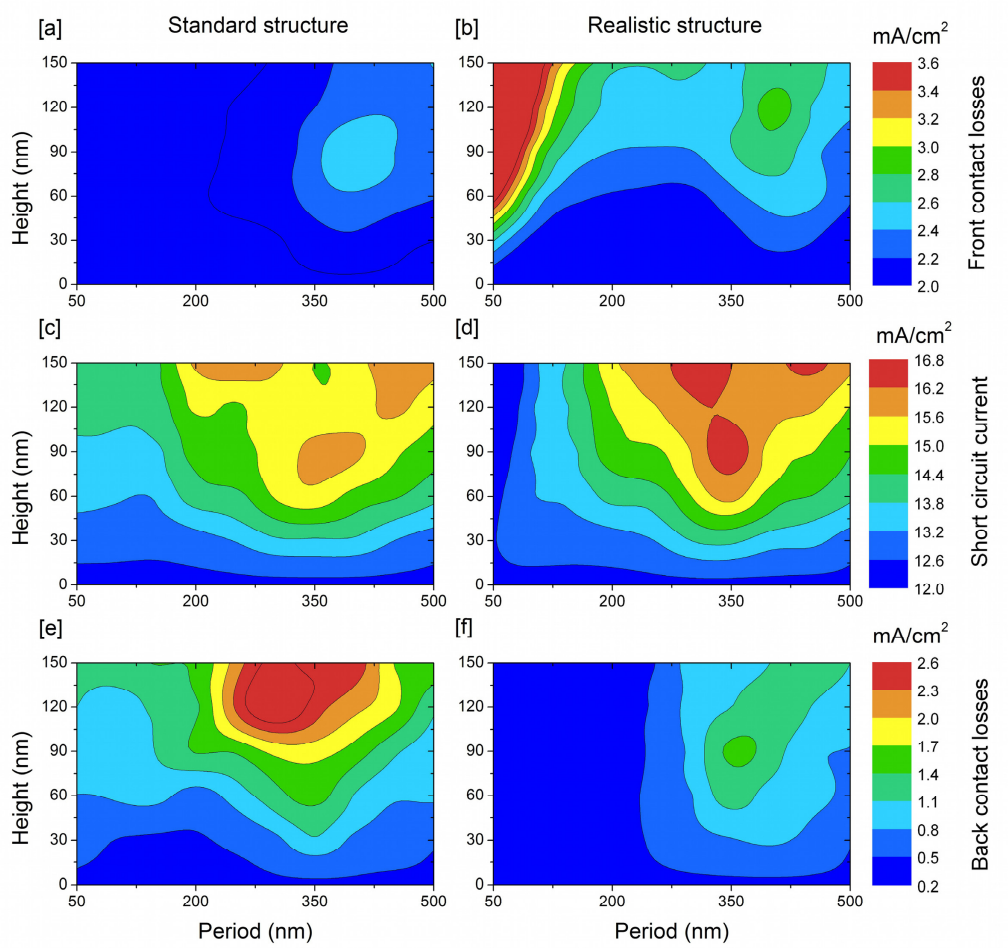

Fig. 8. Comparison of amorphous solar cells with standard and realistic interface morphologies. (a) Front contact losses, (c) short circuit currents and (e) back contact losses for standard solar cell structures as a function of pyramid dimensions. (b) Front contact losses, (d) short circuit currents and (f) back contact losses for realistic solar cell structures.

higher. The differences between standard and realistic structures are smaller for larger periods and smaller heights. The influence of the increased effective thickness of the i-layer on the short circuit currents depends on the light trapping properties of the front and the back contact textures. For the region where the effective thickness of the i-layer is highest [Fig. 3(b)], the short circuit currents for the standard and the realistic structures are almost the same. In other words, increased effective thickness can result in improved short circuit currents only if the front contact and the back contact textures allow for efficient light trapping. The presented results show that the performance of solar cells with periodic surface textures depends on the interface morphology. A realistic description of solar cell interfaces is necessary for accurate investigation and improvement of light trapping.

5. Summary

The influence of realistic interface morphologies on light trapping of periodically textured amorphous silicon thin film solar cells was investigated. The realistic interface morphologies were obtained by using a surface coverage algorithm that assumes film formation in direction of the surface normal. The realistic interface morphologies exhibit significant differences compared to the front contact textures resulting in a reduced roughness of the back contact

#188123 - $15.00 USD Received 1 Apr 2013; revised 29 Apr 2013; accepted 12 May 2013; published 22 May 2013

and an increased thicknesses of the solar cell layers. Optical simulations were used to determine the absorption in the individual solar cell layers. To determine the influence of the realistic interface morphologies on light trapping, the standard solar cell structures with identical front and back contact morphology are used a reference. The amorphous silicon solar cells exhibit high short circuit currents if the height of the pyramid is larger than 90 nm and the period is in the range of 300 nm to 400 nm. For periods smaller than the optimal, the realistic solar cell structures exhibit increased effective thickness of the p-layer and reduced roughness of the back contact. This results in a drop of the short circuit current despite the increased effective thickness of the i-layer. For periods larger than the optimal, the performance of the solar cells with realistic interface morphologies is similar to the standard structures. For optimal periods, the back contact morphology of solar cells with realistic interfaces is smoother compared to the standard solar cells. Consequently, the back contact absorption is lower and the short circuit currents are higher for realistic solar cells. The increased thickness of the i-layer contributes to the short circuit current only if the front and the back contact morphology allow for efficient light trapping. The film formation and the realistic description of the interface morphologies have to be taken into account when optimizing light trapping in silicon thin film solar cells. Realistic description of the interface morphologies is crucial for describing the optics in radial nanowire solar cells or solar cells deposited on double textured substrates.

#188123 - $15.00 USD Received 1 Apr 2013; revised 29 Apr 2013; accepted 12 May 2013; published 22 May 2013